RESEARCH ARTICLE

Microglial morphology in the somatosensory cortex across lifespan. A quantitative study

Sanziana Godeanu[1,2] | Devin Clarke[3] | Laura Stopper[2] |
Alexandru-Florian Deftu[4,5] | Aurel Popa-Wagner[1] | Adrian Tudor Bălşeanu[1] |
Anja Scheller[2] | Bogdan Catalin[1,2]

[1]Experimental Research Centre for Normal and Pathological Aging, University of Medicine and Pharmacy of Craiova, Craiova, Romania

[2]Department of Molecular Physiology, CIPMM (Center for Integrative Physiology and Molecular Medicine), Building 48, University of Saarland, Homburg, Germany

[3]School of Psychology and Sussex Neuroscience, The University of Sussex, Falmer, Brighton, UK

[4]Pain Center, Department of Anesthesiology, Lausanne University Hospital (CHUV), Lausanne, Switzerland

[5]Faculty of Biology and Medicine (FBM), University of Lausanne (UNIL), Lausanne, Switzerland

Correspondence
Anja Scheller, Department of Molecular Physiology, CIPMM (Center for Integrative Physiology and Molecular Medicine), University of Saarland, Homburg, Germany.
Email: anja.scheller@uks.eu

Bogdan Catalin, Department of Functional Sciences, University of Medicine and Pharmacy of Craiova, Craiova, Romania.
Email: bogdan.catalin@umfcv.ro

Funding information
Unitatea Executiva pentru Finantarea Invatamantului Superior, a Cercetarii, Dezvoltarii si Inovarii, Grant/Award Number: TE 150 (PN-III-P1.1-TE-2019-1366)

Abstract

Background: Microglia are long-lived cells that constantly monitor their microenvironment. To accomplish this task, they constantly change their morphology both in the short and long term under physiological conditions. This makes the process of quantifying physiological microglial morphology difficult.

Results: By using a semi-manual and a semi-automatic method to assess fine changes in cortical microglia morphology, we were able to quantify microglia changes in number, surveillance and branch tree starting from the fifth postnatal day to 2 years of life. We were able to identify a fluctuating behavior of most analyzed parameters characterized by a rapid cellular maturation, followed by a long period of relative stable morphology during the adult life with a final convergence to an aged phenotype. Detailed cellular arborization analysis revealed age-induced differences in microglia morphology, with mean branch length and the number of terminal processes changing constantly over time.

Conclusions: Our study provides insight into microglia morphology changes across lifespan under physiological conditions. We were able to highlight, that due to the dynamic nature of microglia several morphological parameters are needed to establish the physiological state of these cells.

KEYWORDS
cortex, lifespan changes, microglia arborization

Sanziana Godeanu and Devin Clarke contributed equally to this work.

1 | INTRODUCTION

As resident immune cells of the central nervous system (CNS), microglia continuously survey their microenvironment.[1-4] Microglia are permanently extending and retracting their processes constantly changing their morphology. This cellular change is rapid. For example, 3-5 minutes of global hypoxia can generate significant microglia morphology alterations.[5] Microglia heterogeneity between different cortical regions, as well as within the same region,[6] makes it difficult to establish morphological difference between physiological and any hypo-arborization that microglia may undergo under early pathological conditions.[7,8] Except for their role in synaptic pruning,[9-12] where morphological changes are a consequence of their phagocytic function, little is known regarding the dynamics of physiological changes of microglia morphology in the CNS[13-15] compared to inflammatory conditions.

Fundamental questions, such as, what is the mechanism that maintains the microglial population across lifespan and what are the cell proliferation dynamics, are still unanswered. Until now the general consensus was, that under physiological conditions, the microglia population is sustained via local clonal expansion throughout life.[16,17] However, some studies suggested that the whole population is slowly renewed several times during one's lifespan[18] by intense cell proliferation with no circulating monocytes/macrophages infiltration.[19] Fate-mapping studies hypothesized that CNS recruited monocyte-derived macrophages can differentiate into the microglial population under certain physiological conditions and retain their unique identity.[20,21] In contrast, after microglial depletion, repopulation is performed by remaining residual microglia, not by peripheral macrophages.[22,23] Depending on the exact way one looks at the microglia population across the lifespan, the described morphological changes generated by age[24] can simply be a consequence of slow proliferation and/or renewal of resident microglia. The age-associated morphological changes have ranged from simple observations regarding variations in soma volume and shortening of microglia processes,[25] to the observation that in some parts of the aged brain microglial bodies move closer together.[19,26] On top of these simple observations, more complex morphological changes have been reported in pathophysiology. While the motility of microglia in young animals increase in response to injury up to 3-fold, in aged animals this increase was not observed.[27]

Besides morphological alterations, some intracellular changes add to the plethora of changes found in senescent microglia. These vary from reports showing accumulation of lipofuscin granules[28] to cytoplasmic fragmentation and iron storage.[29] Other observations also associated with senescent microglia include a decrease in neuroprotective functions, an increase in glutamate-induced neurotoxicity[30] or an altered antigen expression within aged microglia including a higher number of MHC Class II proteins, CD4 and macrophage markers ED1,2,3.[31] Higher level of pro-inflammatory cytokines (TNF-alpha, IL-1beta, IL-18) and lower level of anti-inflammatory cytokines (IL-10, IL-4 or brain-derived nerve growth factor)[32] have also been reported.

A major breakthrough in understanding the level of microglia involvement in the normal physiology of the CNS has been the discovery of their dynamics in vivo[1,2,33] and their direct contacts with neuronal synapses.[34] The direct visualization of microglia in living animals has made us understand that the difference in "activated" and "resting" microglia is much smaller and different from that we thought.

Here, we explored, in depth, the age-related changes in microglia morphology of the mouse somatosensory cortex. We analyzed population parameters such as the number of cells, microglial aggregates and individual cell morphologies. We also provide a detailed analysis of the (1) total length of branch tree, (2) number of branches, (3) mean branch length, (4) number of each branch order and (5) mean area surveilled by each microglia cell. We also compare our results with data generated by a semi-automated method in order to have proper controls. As such, we aimed to define, as accurately as possible, the morphological features of microglia at the analyzed time points.

2 | RESULTS

2.1 | Basic cortical microglia characteristics change with age

As we gain deeper knowledge about microglia physiology, it becomes clear that microglia density, number of microglia with cell bodies in close proximity to one another (indicative of division), area of each cell (quantified as surface area occupied by the cell body and branches as observed from the middle of the cell body) and surveilling area are parameters that are changing constantly under physiological conditions. Moreover, by analyzing these parameters, we can get a better understanding of microglia dynamics across lifespan. Here we found that microglia density differs across lifespan (Figure 1A) ($P < .0001$), with a rapid increase in density in the first 3 weeks of life and a decrease to the lowest number at 20 weeks (8300 ± 2500 cells/mm^3). From 58 weeks of age onwards, microglial density remained
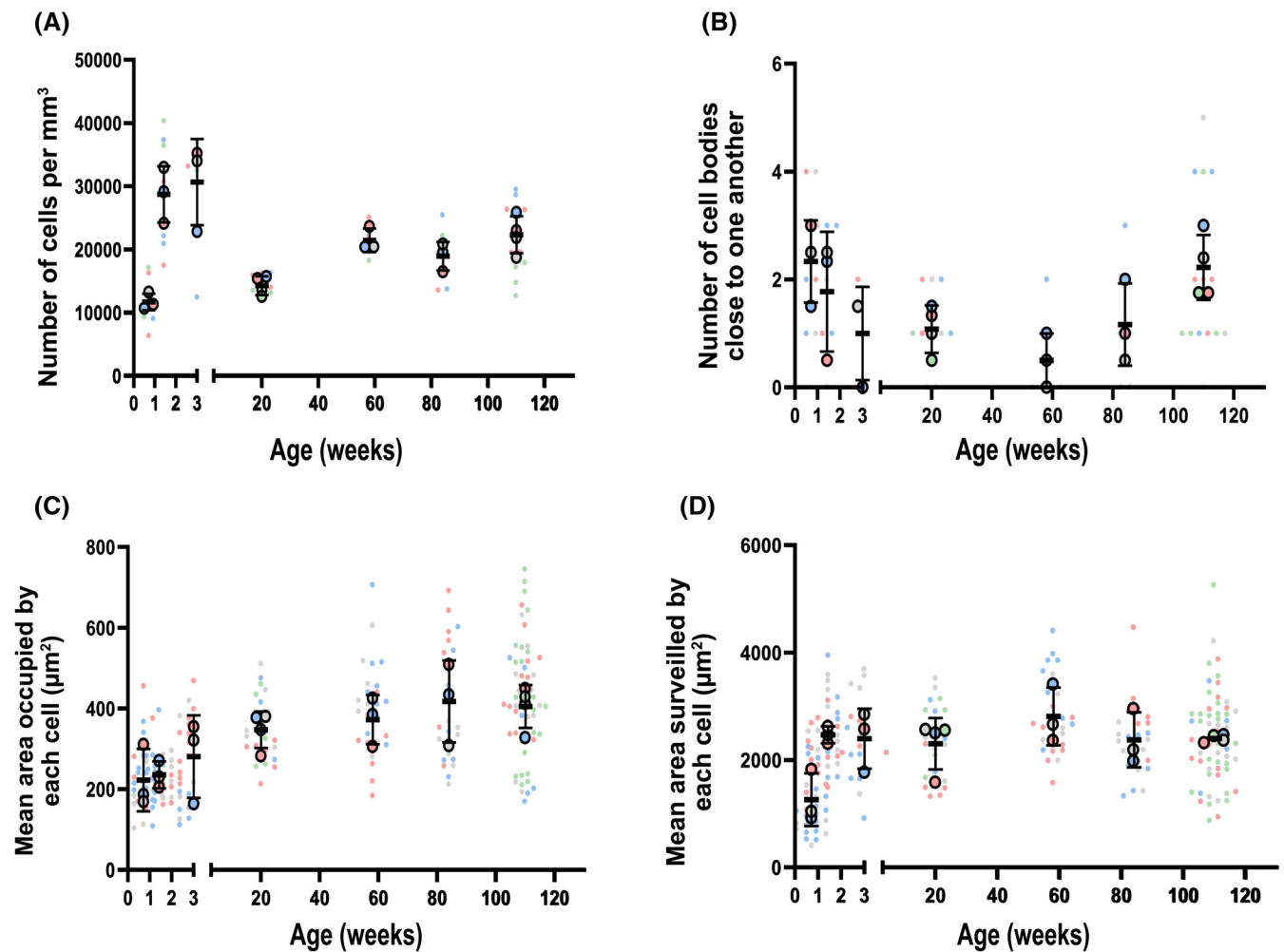
FIGURE 1 Basic microglia characteristics change in an age dependent manner. (A) Microglial density quantified immediately after birth reveals an approximate 3-fold increase in the first 21 days after birth, with decrease in young adults (20 weeks of age) followed by a nearly 2-fold increase in older adults and aged animals. The multiple comparison Turkey test revealed differences between different time point on early life, early and adult life and between different time points of adult life (ANOVA, $P < .0001$, Table 2). (B) Over the analyzed lifespan we observed minimal signs of microglia division, with a slight increase in aged individuals (ANOVA, $P = .0437$, Table 2) suggesting equal proliferation rates. (C) Over time microglia tended to hypertrophy with their bodies and processes occupying larger areas (ANOVA, $P = .0107$), but (D) the average surveilled area for each cell seems to be relatively constant, except directly after birth, where the occupied area was smaller (50% reduction) (ANOVA, $P = .0158$). Each colored circle represents an animal, and the same colored dots represent de analyzed cells from that animal.

relatively stable, with no difference between 58, 84, and 110 weeks of age. Microglia cells do not contact one another under physiological conditions[2,3] and as such, we considered any two microglia bodies close together as signs of apparent division (confirmed by Ki67 staining [Figure 2]). This phenomenon was observed at all analyzed time points with no differences between each age group (Figure 1B) (Table 1). However, the lowest number of microglia cell bodies found in close vicinity was seen at the age of 58 weeks with only 0.5 ± 0.5/mm^3 compared to 2.33 ± 0.76/mm^3 in P5 or 2.22 ± 0.6/mm^3 in 110-week-old mice, indicating age-related proliferation rates. We also determined the mean space occupied by

each cell. We observed a constant increase in the average area occupied by the cells over time (Figure 1C) ($P = .0107$). With microglia cells in the brain of P5 mice occupying on average an area of 222.84 ± 77.22 μm^2 and reaching 417.35 ± 101.54 μm^2 at 84 weeks of age. In very old animals (110 weeks of age), this number started to slightly drop to around 405.18 ± 53.38 μm^2. While the average space occupied by each cell was constantly increasing, the mean area surveyed by each cell seems to vary more. Cortical microglia from P5 mice had the lowest surveilled area (1264.07 ± 489.77 μm^2) as compared to microglia analyzed from 58 week-old mice (2814.69 ± 539.7 μm^2) (Figure 1D) ($P = .0158$).
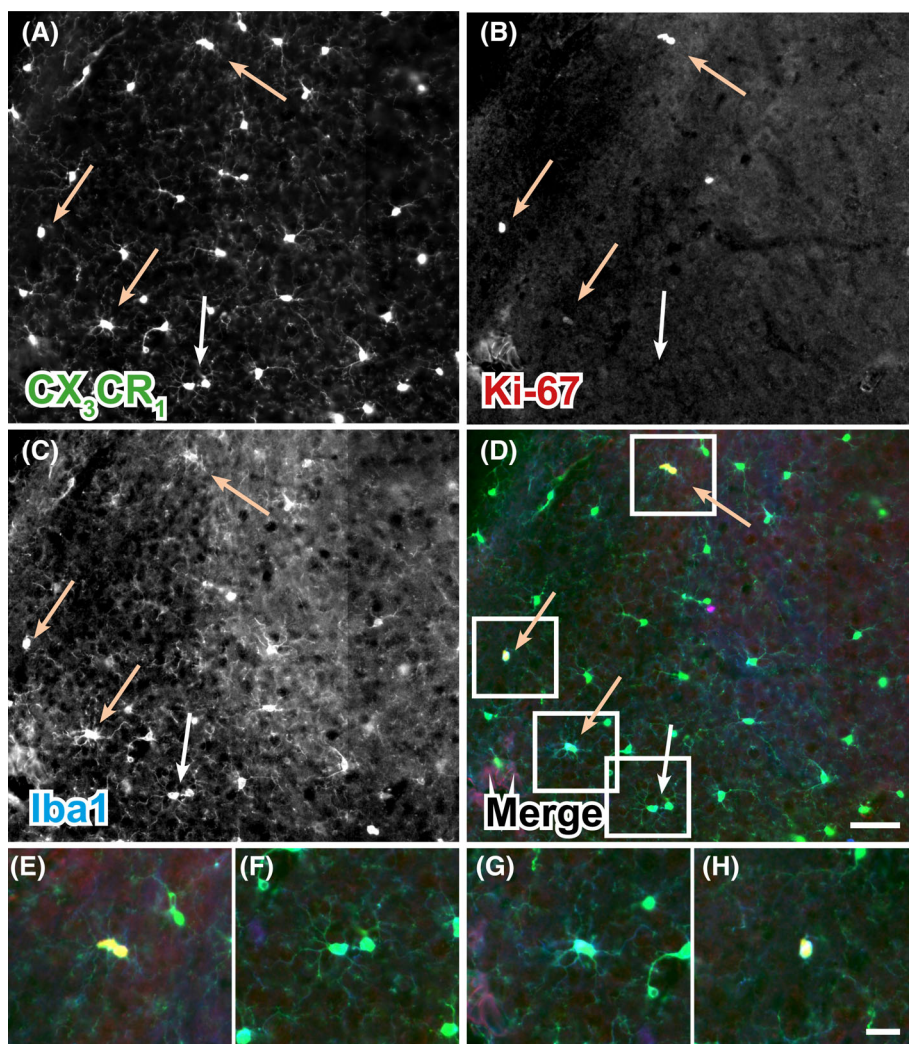
FIGURE 2 Example of Ki-67 staining in the cortex of a 20-week-old animal highlighting microglia division in the cortex. (A) Microglia of CX3CR1-EGFP mice overlap partially with Ki-67 (B) and perfectly with Iba1 (C) staining. (A-D) Yellow arrows indicate Ki-67 positive microglia in different stages of division. The white arrow indicates microglia bodies abnormally close, probably in the G1 or G0 phase, for which Ki-67 has a low affinity. (E-H) Magnifications of Ki-67 positive and negative microglia highlighted the respective arrows in A-D. Scale bar in A-D: 50 μm, in E-H: 20 μm.

2.2 | Microglia morphology is subjected to fluctuating changes with age

By closely tracing the arbor of individual cortical microglia, we were able to evaluate microglia morphology changes that occur in the healthy mouse cortex over time. The parameters used in these detailed analyses are: (1) the total length of the branch tree, (2) the number of branches, (3) the mean branch length, and (4) cataloguing the number of each branch order. They revealed an age-related morphology of microglia, with dynamic changes appearing in early life but also during different ages in adult mice (Table 1). Immediately after birth, microglia display a rather small arbor, with a total length of 178 $\pm$ 53.22 μm. However, this increases fast, reaching 562.15 $\pm$ 171.23 μm around 21 days of age. This total length is kept almost constant until one and a half years of age (84 weeks), the lowest length of adult life (418.14 $\pm$ 28.53 μm). At 2 years of age (110 weeks), the arbor starts to increase again to 507.93 $\pm$ 48.14 μm (Figure 3A) ($P = .0002$). A similar trend was observed when the

number of microglial branches was evaluated. The highest number of branches was reached around 20 weeks of age (126.27 ± 15.14) (Figure 3B) ($P = .0002$). With the total length of the branch tree varying over time, the mean branch length was relatively constant around 5.64 $\pm$ 0.6 μm (Figure 3C). The only change in the mean length of a microglia branch seems to be between younger and older adults, with younger animals having shorter (4.76 ± 0.2 μm in 20 weeks of age mice) mean branch length than aged ones (6.4 ± 0.37 μm in 84 weeks of age mice) (Figure 3C) ($P = .0014$).

Aging induces different changes in the number of microglia branches according to their branch order. Visual inspection of the isolated cells revealed a difference between microglia branches at different ages (Figure 4). By classifying each branch within a cellular tree, we were able to identify morphological differences across lifespan. The number of primary microglia branches remained stable throughout the lifespan of a mouse (Figure 5A; 3.1 ± 0.2 primary branches; $P = .1025$). The most important morphological

TABLE 1   Mean values of all parameters obtained by semi-manual method of quantifying microglia morphology.

| Analyzed parameter | Age | | | | | | | | | | | | | |
	Days						Weeks							
	5		10		21		20		58		84		110	
	Mean	SD	Mean	SD	Mean	SD	Mean	SD	Mean	SD	Mean	SD	Mean	SD
Microglia density	11 722.18	1324.97	28 741.07	4450.91	30 674.95	6824.66	14 298.83	1482.74	21 470.56	1853.44	18 953.06	2258.68	22 348.38	2941.82
Cell apparent division	2.33	0.76	1.78	1.11	1.00	0.87	1.08	0.44	0.50	0.50	1.17	0.76	2.23	0.60
Mean area	222.83	77.23	235.82	33.21	280.85	101.98	347.67	45.47	372.50	60.97	417.36	101.54	405.18	53.38
Mean arbor area	1264.07	489.77	2470.14	156.92	2399.59	561.26	2303.59	479.60	2814.69	539.70	2378.31	512.46	2404.67	69.75
Total length	178.14	53.23	482.02	84.12	562.15	171.23	600.08	74.66	578.94	74.42	418.15	28.54	507.93	48.15
Number of branches	30.92	36.28	90.28	27.15	105.80	32.41	126.28	11.99	93.62	15.87	65.77	9.04	98.40	8.44
Mean branch length	6.01	0.42	5.50	0.69	5.41	0.34	4.76	0.28	6.27	0.72	6.40	0.37	5.13	0.17
Branches														
Primary	3.00	0.15	2.94	0.40	3.03	0.31	3.41	0.18	3.00	0.11	2.96	0.44	3.40	0.18
Secondary	5.83	0.71	7.03	1.18	7.43	0.97	9.80	1.34	7.88	0.33	8.19	1.45	8.73	1.24
Tertiary	6.59	2.04	10.90	2.01	13.73	1.63	16.28	0.90	13.15	1.20	12.39	2.15	14.06	1.79
Quaternary	5.69	1.49	14.00	2.29	17.63	3.81	18.23	1.36	16.14	0.67	13.54	1.37	15.77	2.16
Terminals	11.19	6.21	47.47	10.50	63.87	30.09	78.22	17.31	52.88	13.75	28.44	4.21	56.35	3.90
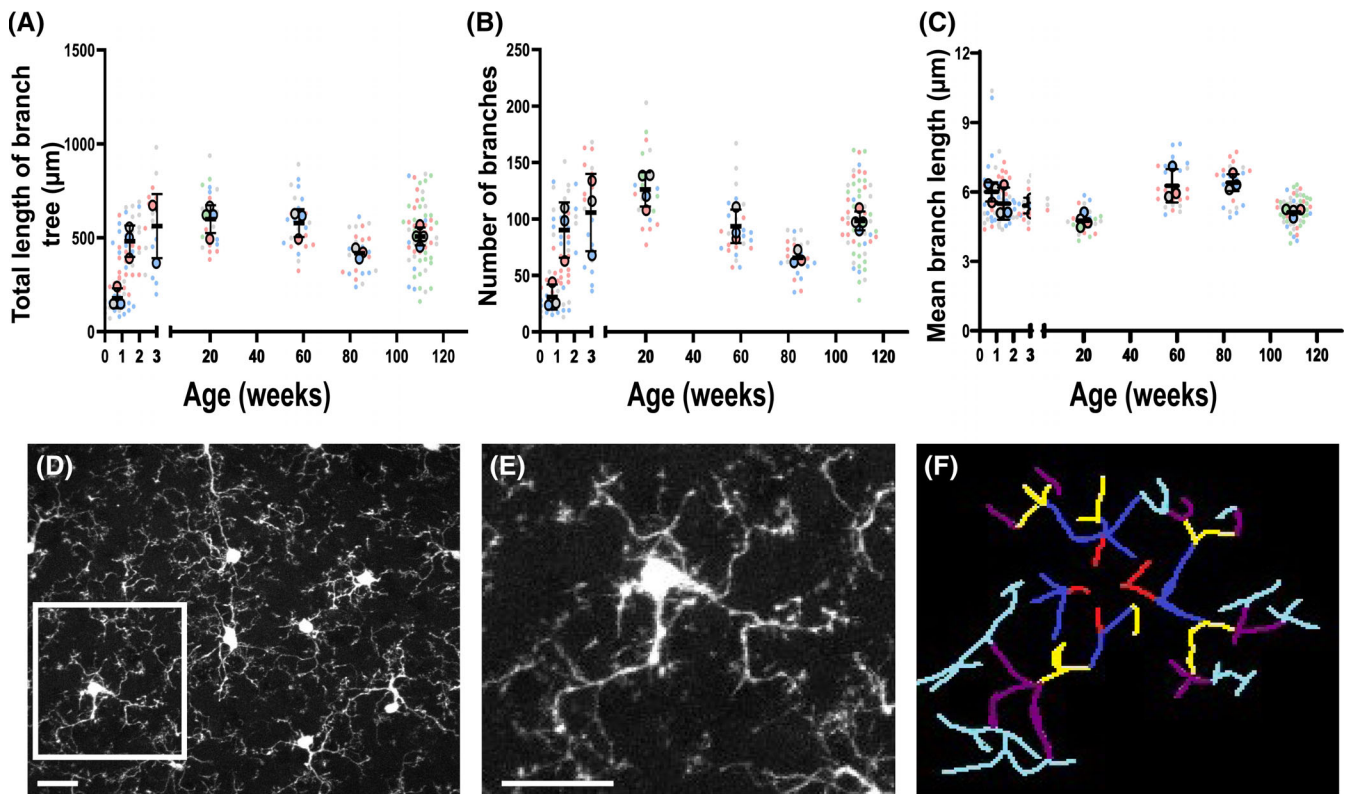
FIGURE 3 Basic microglia arbor morphology changes across lifespan. By tracking each branch and its order, we were able to generate a complete and detailed image of the morphological variations that microglia overcome over time. (A) Although the total arbor length of microglia is stabilized after 10 days of age (around 550 μm), (B) changes in the number of branches generate differences between young adult and older adult mice, with individual microglia analyzed for young animals displaying a greater dispersion in the number of individual branches (36.86%) compared with cells analyzed in other adult time points (around 27%). (C) The mean branch length is the parameter that showed the highest number of differences within the adult life, with the average length of older adults (6.4 ± 0.3 μm) being significantly larger than both young adults (4.7 ± 0.27 μm) and aged animals ((5.1 ± 0.17 μm) (multiple comparison Tukey $P < .01$, respectively, $P < .05$). (D) Example of confocal cells in maximum projection, (E) from which a single cell was isolated and (F) analyzed by counting the number and length of each order of branches. The red ones are considered primary branches, as they are leaving the microglia body, the dark blue ones are secondary, as they are formed from primary ones, yellow are tertiary, purple quaternary and light blue are terminal branches. Scale bar 20 μm. Each colored circle represents an animal and the same colored dots represent de analyzed cells from that animal.

distinction, that is, that the microglia arbor undergoes changes with advanced age, is associated with secondary, tertiary and quaternary branches. The tendency is the same in this order of branches, but slight differences can be observed. For example, the numbers of secondary, tertiary and quaternary branches are increasing in the first few weeks of life, but the maximum number of each branch order is reached at different time points. While the secondary (9.8 ± 1.34) and tertiary (16.27 ± 0.9) ones reach a clear maximum at 20 weeks of age, the maximum number for the quaternary branches is already reached at 21 days after birth, remaining high until 20 weeks of age and slowly decreasing until 58 weeks of age (16.14 ± 0.67 compared to 17.63 ± 3.8 and 18.23 ± 1.36; Figure 5B-D; Table 1). As expected, the most dynamic order of branches were the terminal branches. In early life, microglia have a low number of terminal branches, with an average of 11.18 ± 6.21 branches per cell at P5. However, the number of terminal branches was the only one changing in adult life. While a young adult (20 weeks of age) had around 78.21 ± 17.3 terminal branches, this number dropped constantly across lifespan, reaching the lowest value around 84 weeks of age (28.44 ± 4.21). Beyond this age, the number of terminal branches started to increase, reaching 56.34 ± 3.89 at 110 weeks of age (Figure 5E).

2.3 | Automated analysis confirms manual findings

A manual approach to the morphological analysis requires lot of work and therefore is often limited in terms of number of cells that can be quantified and

FIGURE 4 Exemplification of microglia analyses across lifespan. Heterozygotes CX3CR1+/− mice were used in the morphology study. These animals were randomly chosen to be analyzed at the age of 5 (n = 3), 10 (n = 3), and 20 (n = 3) days after birth, and 21 (n = 4), 58 (n = 3), 84 (n = 3), and 110 (n = 4) weeks of age, respectively. All microglia were recorded using confocal imaging from the somatosensory cortex of the mice. Individual microglia were isolated from the original stack, skeletonized, and the surveyed and occupied area were manually done.
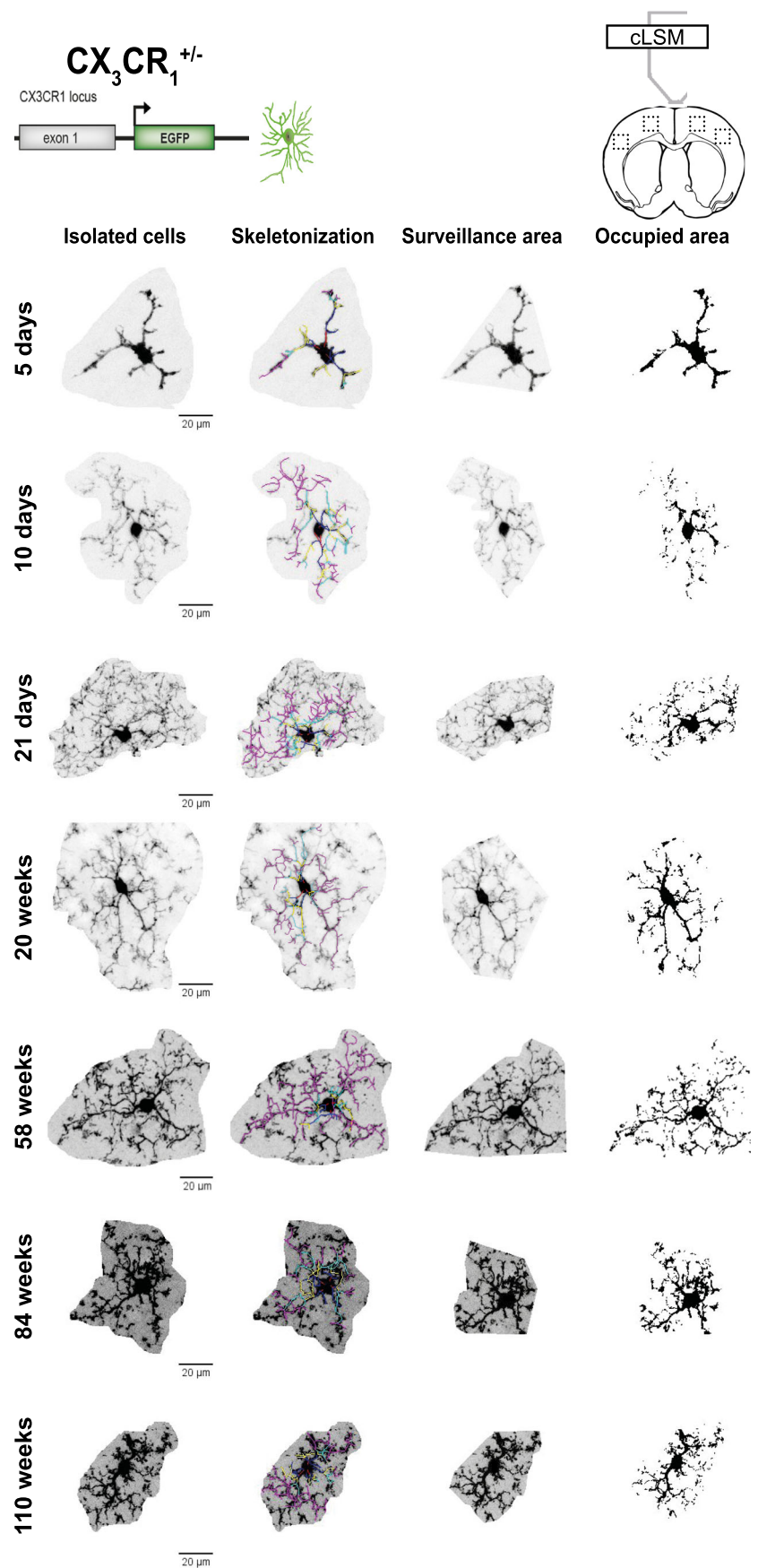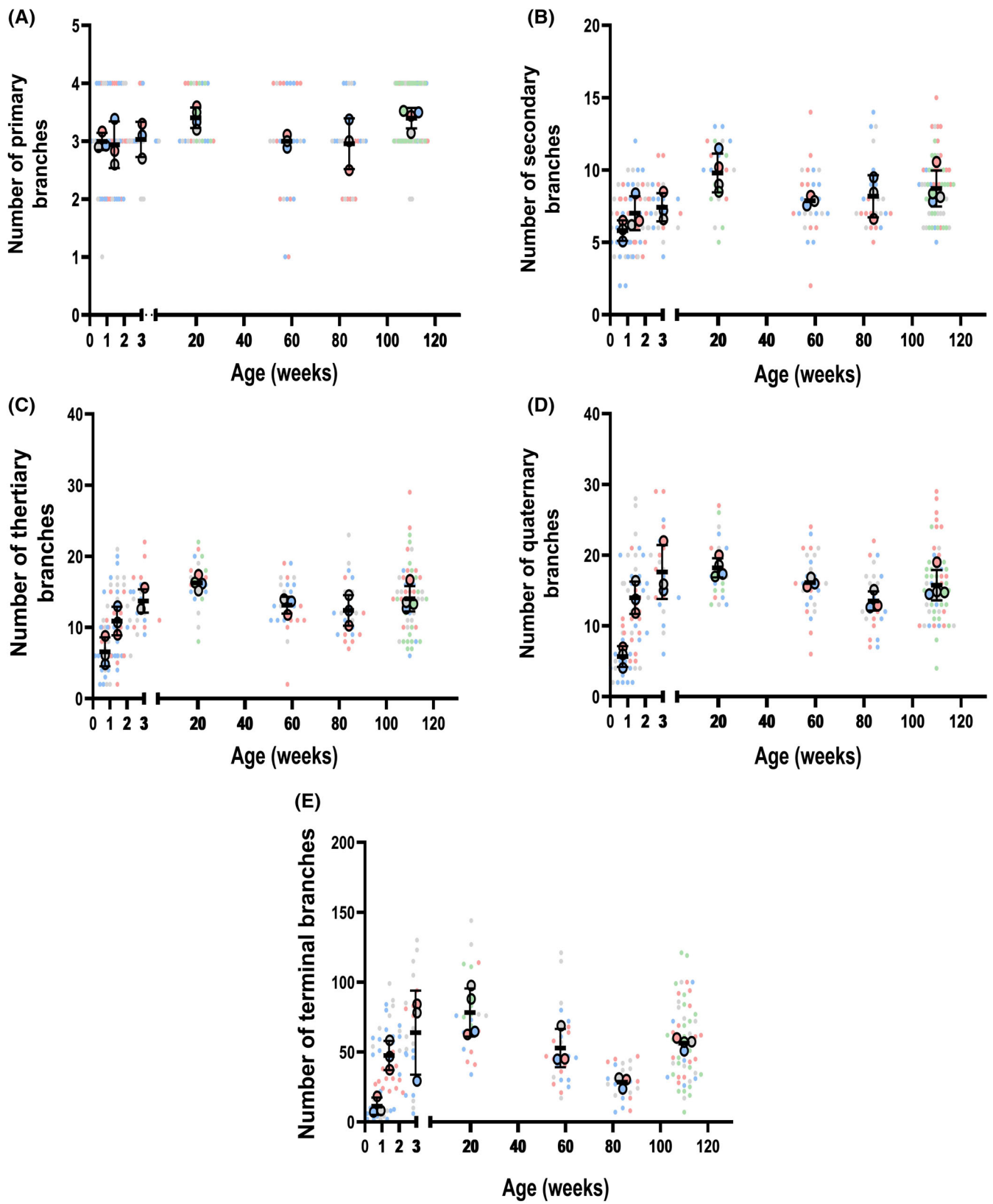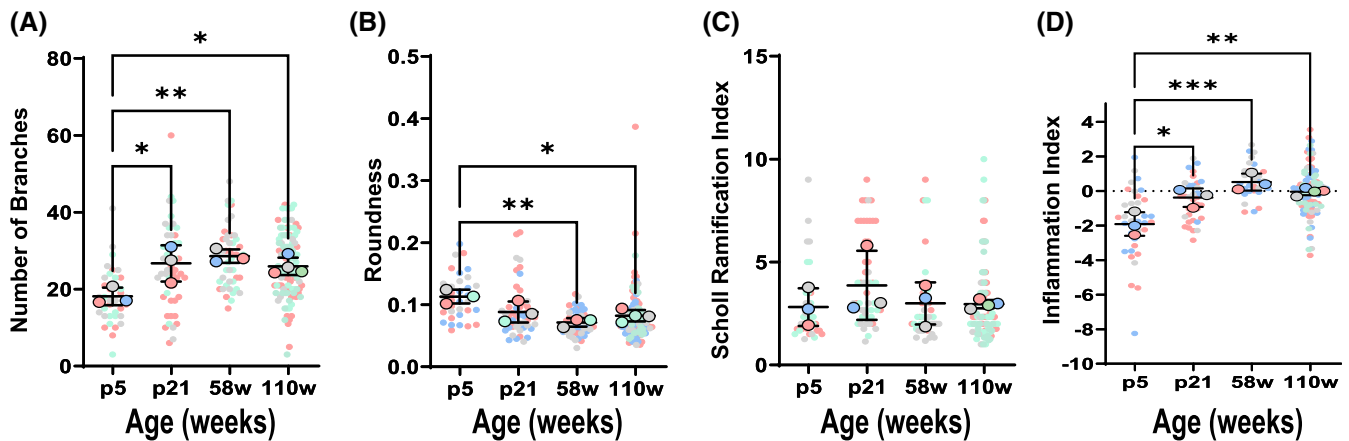
FIGURE 5   Legend on next page.

FIGURE 6 Semi-automated method quantifying microglia morphology confirms manual findings. Our semi-automated morphology analysis detected (A) an increase in branch number between P5 (18.13 ± 2.28) and 110 weeks (25.95 ± 2.26) ($P = .001$). We also observed that when constructing our composite morphology metric (Inflammation Index) both (B) roundness and (C) the Sholl ramification index were selected as useful features for discriminating between 58 weeks (roundness 0.071 ± 0.0069; ramification index 3.00 ± 1.02) and P21 (roundness 0.088 ± 0.017, $P = .004$; ramification index 3.87 ± 1.68, $p = .022$). Utilizing the Inflammation Index (D), we confirmed a difference in overall morphology between P5 and 110 weeks ($F (1, 5) = 28.111$, $P = .003$) and no difference between P21 and 58 weeks ($F (1, 4) = 4.593$, $P = .099$), agreeing with the results of the manual analyses. However, the presence of difference in individual morphology metrics between P21 and 58 weeks, coupled with the Inflammation Index P value passing trend level, provided weak evidence there may be a morphological difference between the two timepoints. Each colored circle represents an animal and the same colored dots represent de analyzed cells from that animal.

compared. In addition, the corrections for multiple statistical tests required, when evaluating numerous aspects of morphology, restrict statistical power and the ability to detect smaller effect sizes. By employing an automated approach (the "Inflammation Index" duo of packages[35]) we were able to measure 43 different metrics for each cell and combine a selection of these into a composite metric that simply measures morphological change. As positive control, we first evaluated the ability of the automated technique to identify morphological differences identified using our manual analysis. We compared data collected at P5 and 110 weeks, where differences were found for the number of branches (Figure 6A), mean branch length, and mean arbor area (Table 2). With the automated approach, we were able to construct a composite metric that showed a difference between P5 and 110 weeks using a TMS (Target

Mask Size) of 300 μm^2 (110 weeks n = 4 animals; P5 n = 3 animals; $F (1, 5) = 28.111$, $P = .003$), indicating a difference in morphology between these time points. Of note, the automated analysis identified mean branch length as a good metric for inclusion in the composite value, in agreement with the manual analysis. While the number of branches was not included in the composite value, there was an increase in branch number from P5 to 110 weeks in the automated data set (110 weeks n = 4 animals; P5 n = 3 animals; $F (1, 5) = 20.381$, $P = .006$). There was no similar measurement to mean arbor area included in our automated analysis. Interestingly, cell spread (which measures the average distance from the center of mass of the cell mask to its four extremities) was included in the composite metric, suggesting changes occur in cell polarity between these time points (Figure 6C).

FIGURE 5 Detailed analysis revealed oscillations in microglia morphology over time. With most of the other branch order suffering changes over the lifespan of the mice, (A) the first order branch number remains constant across all analyzed time points. (B) The number of secondary order branches seems to only differ from P5, where the lowest numbers of secondary branches (5.82 ± 0.7) can be seen, compared to 20 weeks (9.8 ± 1.33) (ANOVA, $P = .004$) and 110 weeks (8.7 ± 1.24) (ANOVA, $P = .049$). (C) The highest number of differences between early and adult life microglia morphology was observed in the number of tertiary branches, with (D) quaternary ones following closely in the same category (ANOVA, $P < .0001$). (E) The only difference between the number of branches in the adult life was recorded in the terminal branches, where cortical microglia quantified in young adult mice presented with more terminal branches (78.21 ± 17.31) compared to 84 weeks mice (28.44 ± 4.21) (ANOVA, $P = 0.006$). Each colored circle represents an animal and the same colored dots represent de analyzed cells from that animal.

TABLE 2 Values obtained in both ANOVA and Tukey multiple comparison test.

ANOVA multiple comparison Tukey

			Early life			Early vs adult life												Adult life					
	P value	R square	5 vs 10	5 vs 21	10 vs 21	5 vs 20	5 vs 58	5 vs 84	5 vs 110	10 vs 20	10 vs 58	10 vs 84	10 vs 110	21 vs 20	21 vs 58	21 vs 84	21 vs 110	20 vs 58	20 vs 84	20 vs 110	58 vs 84	58 vs 110	84 vs 110
Microglia density	<.0001	.8814	***	****	ns	ns	*	ns	*	***	ns	*	ns	***	ns	**	ns	ns	ns	ns	ns	ns	ns
Cell apparent division	.0437	.5171	ns	ns	ns	ns	ns	ns	ns	ns	ns	ns	ns	ns	ns	ns	ns	ns	ns	ns	ns	ns	ns
Mean area	.0107	.6078	ns	ns	*	ns	ns	ns	*	ns	ns	ns	ns	ns	ns	ns	ns	ns	ns	ns	ns	ns	ns
Mean arbor area	.0158	.5852	*	ns	ns	ns	**	ns	*	ns	*	ns	ns	ns	ns	ns	ns	ns	ns	ns	ns	ns	ns
Total length	.0002	.7748	**	***	ns	***	***	**	**	ns	ns	ns	ns	ns	ns	ns	ns	ns	ns	ns	ns	ns	ns
Number of branches	.0002	.7808	*	**	ns	****	**	ns	**	ns	ns	ns	ns	ns	ns	ns	ns	**	**	ns	ns	ns	ns
Mean branch length	.0014	.7059	ns	ns	ns	*	ns	ns	ns	*	ns	ns	ns	ns	ns	ns	ns	**	**	ns	*	*	*
Branches																							
Primary	.1025	.4474	ns	ns	ns	ns	ns	ns	ns	ns	ns	ns	ns	ns	ns	ns	ns	ns	ns	ns	ns	ns	ns
Secondary	.0083	.6222	ns	ns	ns	**	ns	ns	*	*	ns	ns	ns	ns	ns	ns	ns	ns	ns	ns	ns	ns	ns
Tertiary	<.0001	.8005	**	**	ns	****	**	**	***	ns	ns	ns	ns	ns	ns	ns	ns	ns	ns	ns	ns	ns	ns
Quaternary	<.0001	.8313	****	****	ns	****	***	***	***	ns	ns	ns	ns	ns	ns	ns	ns	**	ns	ns	ns	ns	ns
Terminals	.0006	.7403	**	**	ns	***	*	ns	*	ns	ns	ns	ns	ns	ns	ns	ns	ns	ns	ns	ns	ns	ns

Abbreviation: ns, nonsignificant.

****$P < .0001$; ***$P < .001$; **$P < .01$; *$P < .05$.

As a next step, we wanted to see if we could construct a metric that distinguished between time points where manual analysis had identified no morphological difference, to investigate if the lack of difference was due to the metrics chosen for manual analysis. Here we compared P21 to 58 weeks. In this case the "Inflammation Index" was unable to construct a composite metric that showed a significant difference between the time points at any TMS value, including 300 μm²; the size at which differences were detected between P5 and 110 weeks (58 weeks n = 3 animals; P21 n = 3 animals; $F(1, 4)$ = 4.593, $P = .099$) (Figure 6D). While on one hand this signals agreement with the manual approach, the P value in this analysis did pass trend level, providing weak evidence that a difference may exists but suggesting that this study may be underpowered to detect it. The metrics identified to best discriminate between p21 and 58 weeks were the roundness of the cell mask (Figure 6C) and the Sholl ramification index. This suggests that if morphological differences exist between these time points, they are perhaps more subtle than what we chose to measure manually.

3 | DISCUSSION

Under physiological conditions, CNS microglia, unlike other macrophages, exhibit a ramified morphology, with each cell covering its own territory which is permanently scanned a few times per day.[2] However, slight changes in their environment generate significant morphological changes.[5] In order to perform continuous surveillance, microglia need to adapt their morphology.[1-3,36] This dynamic change takes place constantly over their lifetime[37,38] and is under physiological conditions subjected to both short- and long-term remodeling. Immediately after birth, the microenvironment of the cerebral cortex changes from a rapid-developing environment with many proliferating and migrating cells[39,40] to a mature environment in which microglial characteristics also change. Microglia are the primary immune cells of the CNS and even under physiological conditions, their morphology is linked to changes in their surroundings.[1-3] They will display changes starting from polarized morphologies via rounded cell bodies all the way to amoeboid shape upon detecting tissue damage.[15,41,42] Also, in the presence of amyloid beta in the parenchyma microglia can display less branching and a reduced arborized area[7] and will cluster around blood vessels in case of a blood barrier disruption.[43] As such, determining the exact microglia morphology at a certain age can provide insights into the overall homeostasis of the CNS, as any change in the microenvironment of the cells will be detected and a morphological remodeling will occur. Establishing the

microglia characteristics at different ages will help to better understand the developmental and aging changes that these cells will go through with time. Here, we were able to catalogue detailed morphological changes that microglia undergo throughout their lifetime. By estimating the cortical density of microglia, we determined a dynamic shift in microglial number between different age groups (Figure 1A). Our data show an increase in microglial density in the first 21 days, consistent with previous findings, where the density of microglia increased until day 14 in the brains of mice.[44] The 2 weeks peak is followed by a 50% decrease in microglial numbers to around 14 268.83 ± 1483 cells/mm^3. This drop is also described by other researchers,[45] with reports showing that the density of microglia remains this low for at least 9 months.[46] Our data support this tendency, showing that the values are more than two times lower, when comparing microglia density of young adults (14 268.83 ± 1483 cells/mm^3) with the one found at 21 days of age (30 674.95 ± 6825 cells/mm^3) (Figure 1A). After this drop in density, we confirm previous data showing that the number of microglia tends to increase in older animals,[25,26] but maintaining relatively uniform values, with the number recorded at 58 weeks not different as compared with 84 and 110 weeks of age (Table 1). By tracking the number of cortical microglia from day 5 to 110 weeks of age, we identified two turning points in microglia density. One in the early postnatal development (21 days) with the maximum microglia density (30 674.95 ± 6825 cells/mm^3) and a minimum number for the adult life around 20 weeks of age, followed by a steady increase thereafter. There could be different explanations for the changes in young and aged animals. In young animals, the early proliferation might be a consequence of the high number of microglia needed for synaptic pruning. In older mice, the proliferation might be an indirect consequence of age-induced dysfunction of the blood-brain barrier (BBB).[47] We know now that BBB changes associated with aged can have also pathological causes such as infections,[48] lifestyle[49,50] or even neurodegenerative pathologies.[51] Regardless of the cause of BBB disruption in the aged cortex, there is an imbalance of molecular transport from the parenchyma to the blood, creating a pro-inflammatory environment that highlights the need of an increase of microglia density.

Microglia do not contact each other under physiological conditions and rapidly retract their processes when contact is established.[2,3] Using mice without any obvious pathology, we estimated the microglia proliferation rate by counting the number of cell bodies close to one another. We were able to confirm that this phenomenon is relatively scarce, confirming the low proliferative rate previously reported.[38] However, we were not able to find aggregates of microglia between 18 and 24 months, as previously described.[19,27,52] We only observed a slight increase in the number of microglia (Figure 1A) and of microglia with cell bodies close to each other (Figure 1B) together in the aged cortex.

Certain microglia characteristics such as cellular density, apparent proliferation and mean area occupied by each cell, change across lifespan. However, others like the mean area surveilled by each cell remains relatively the same across all analyzed time points (Figure 1A-D) (Table 1). Aged microglia are subjected to all sorts of signaling molecules that change their morphology and function.[53] Although, we expected the morphology of aging microglia to resemble the one in activated microglia displaying a dysfunctional, altered phenotype, we did not find any signs of senescence within our data.[54]

Regarding the complexity of microglial branching pattern in each age group, the increase in the branch number, observed in young adults, seems to be the outcome of the increase in second, third, fourth and fifth order branches. The total number of branches is lowest at 84 weeks of age (65.77 ± 9.04, Figure 3B). Around this time point, the lowest number of each branch order can be seen, and the trend is true for all analyzed branch orders, except the second that reaches the lowest point already at 58 weeks of age (Figure 5A-E). Between one and one and a half years of age, microglia had fewer processes and a decrease in the total length of the branch tree (Figure 3A,B), morphologically showing similarities with microglia branch shortening seen in the early stage of their activation (Figure 4).[55] Our morphological analysis highlighted also changes in the number of branches of young adults (20 weeks of age) and aged animals (84 weeks of age) with most microglia in the 84 weeks old animals appearing almost deramified compared to young ones, especially regarding the terminal branches (Figure 5E). However, in very old mice, the mean branch length is starting to decrease, probably due to the increase in the number of fifth order processes. The detailed morphological dynamic of microglia has revealed insights on how we should view nonpathological microglia morphology in different age groups.

While all studies on microglia describe the dense arborization in microglia, most of them reported these findings on young adult animals. At this age, microglia display a distinct ramified morphology, with processes that allow them to efficiently scan the microenvironment and with a spatial domain that has reached maturity. While the total length of this arbor and the mean number of branches do not change over time after 10 days of age (Figure 3A,B), the mean branch length seems to display the greatest differences (Figure 3C and Table 1).

To validate our findings, we used the "Inflammation Index" semi-automated duo of packages to analyze

microglia morphology data at four time points: P5, P21, 58 weeks, and 110 weeks. This allowed us to verify the semi-manual approach. Our results showed an overall agreement between the two methods and emphasized the utility of the automated tools particularly considering the strongly reduced time investment. The metrics identified by the automated analysis that proved most useful in distinguishing between microglia morphology at different time points (including mean branch length and cell spread) were similar to those that showed significant differences in our manual analysis when comparing P5 and 110 weeks. Considering that the automated tool had 43 metrics to choose from, this is an encouraging result. It is worth mentioning, however, the inconclusive data provided by the automatic comparison of P21 and 58 weeks. These suggest that more subtle morphological aspects may differ at these time points, such as the roundness of cells. This suggests that a follow-up study should be conducted with larger sample size and a more comprehensive measurement of morphological changes.

An important point about our automated analysis is that we used the same data set to train and test our "Inflammation Index." This means we built a metric to be most sensitive to the very data used to build the metric. As such, we emphasize that the automated results are only exploratory, and a larger confirmatory study, designed for explicit use with this automated tool, with separate training and testing data sets as well as a larger sample size amongst other considerations, must be conducted for these automated results to stand independently of the manual analyses they were compared to.

Due to the constant increase in the average area occupied by each cell (from less than 230 μm² in P5 to more than 400 μm² in 84 weeks of age), all observed differences could be caused by cytoplasmic hypertrophy usually accompanying activation (documented in a large mass of studies that implement rodent models of acute CNS injury).[41,56-59] This process has largely been unseen in the aged human brain where changes like tortuosity of processes and cytoplasmic fragmentation are more frequent.[7,60-62] For 110 weeks animals, the discrepancy between decreasing area occupied by each cell (405.18 ± 53.38 μm²) and decrease mean total length (507.93 ± 48.15 μm), could be interpreted as a sign of microglia losing their functionality. Subsequently, it has been noted that this microglial functional loss is likely to represent a final stage in the neurodegenerative process, with an extraordinary heterogeneity in its morphological appearance.[63] Microglial activation, in response to amyloid plaques, aggravates this process.[64] Whether this decreased ramification alters the potential of microglia to cover the entire brain parenchyma with subsequent incomplete immune surveillance in the aged brain, remains to be determined. Consistent with our findings, age-related changes in microglia morphology were observed in various CNS locations, including the mouse retina,[27] mouse visual and auditory cortex,[26] and somatosensory cortex.[25] In human studies, the same changes were observed by analyzing microglial cells in inferior temporal cortical grey matter with even higher abnormalities in aged AD patients.[7] This increase could be seen as an attempt by microglia to maintain some homeostatic state, as a significant decrease in microglia's "spatial domain" was found in another study focused on the somatosensory cortex.[25] This was not the case in our study as the area surveilled by each cell did not vary across adult life (Figure 1D).

Senescent microglia may be seen as a direct consequence of the aging process and are doubtlessly either responsible for neurodegeneration, or a consequence of neurodegeneration itself. Although aging impairs microglia functions[63] by altering the expression of different membrane proteins[53] directly impacting their activity,[59] it is not clear if this process is age related or it is a consequence of an added neurodegenerative process. Since age-associated damages in the microenvironment can lead to enhanced Ca^{2+} signaling in aging microglia such molecular changes may be also caused by neurodegeneration.[65,66] Furthermore, systemic age-related changes such as metabolic disorders or cardiovascular diseases may influence microglia behavior with time.[67] No cell escapes the undesirable effect of aging. Our study supports the idea that microglia are affected directly by aging and allows a better morphological characterization of microglia throughout life.

Studying microglia morphology can lead to a greater understanding of CNS pathologies as microglia is in one way or another recruited in response to all alterations of the CNS. However, before understanding microglia changes in pathology, we need to first establish how microglia are involved in brain physiology. Due to the constant remodeling of microglia, their morphology is changing all the time. By characterizing microglia morphology in different aged mice, we were able to generate a pattern of the microglia appearance starting with the postnatal period (5, 10 and 21 days after birth), to young adulthood (20 weeks of age) all the way to early (58 and 84 weeks of age) and old aged (110 weeks of age) animals.

4 | EXPERIMENTAL PROCEDURES

4.1 | Animals and experimental groups

In order to obtain the experimental animals, heterozygous transgenic TgH(CX3CR1-EGFP)[68] mice were bred.

The pups of three males and twelve females were used in this report. All CX3CR1−/− (n = 11) and CX3CR1+/+ (n = 20) animals were excluded from the present study. Only CX3CR1+/− animals (n = 23) were used for the morphological comparisons. After confirming the genotype CX3CR1+/− pups (age: 5 (2 males and 1 female), 10 (1 male and 2 female), and 21 (2 male and 1 female) days) were randomly selected for image acquisition. The remaining CX3CR1+/− littermates were analyzed at 20 (2 males and 2 female), 58 (1 male and 2 female), 84 (2 male and 1 female), and 110 (1 male and 3 female) weeks of age (Figure 4). For the immunohistochemistry additional three CX3CR1+/− mice were used. All mice were maintained in C57BL/6N background and on a 12-hour (h) light/dark cycle at 20°C. Transgenic mice were housed in individually ventilated cages in the Animal Facility of the University of Medicine and Pharmacy of Craiova (UMFCV) and fed standard diet ad libitum.

For microglial analysis, mice were perfusion-fixed followed by an overnight fixation to prevent microglial arborization changes documented in other studies, when fixation was conducted without a prior fixative perfusion.[5] Briefly, after intraperitoneal ketamine/xylazine (ketamine 100 mg/kg; xylazine 10 mg/kg) anesthesia and upon cessation of reflexes, mice were transcardially perfused with phosphate-buffered saline (PBS) followed by 4% paraformaldehyde (PFA, pH 7.4 in PBS pH 7.4, 0.1 M). Brain extraction was followed by overnight fixation in PFA 4% at 4°C. All experiments have been conducted according to The Federation of European Laboratory Animal Science Associations (FELASA) guidelines and have been approved by the Wellbeing of Experimental Animal Committee of the UMFCV (no 1.16/10.10.2019) and renew by the Veterinary Sanitary and Food Safety Directorates of Dolj county (14/29.03.2022), according to Romanian, German and European laws.

4.2 | Immunohistochemistry and Image acquisition

After fixation, 40 μm slices were prepared in ice-cold PBS using a Leica VT1000S vibratome (Leica Biosystems, Wetzlar, Germany). The obtained sections were kept at room temperature for 1 hour in blocking solution (1× PBS containing 0.3% Triton X-100 and 5% normal horse serum). Sections were washed three times (1× PBS) for 10 minutes and were placed in a water bath and mounted in Aqua poly mount (Polysciences, Polysciences, Illinois). Sections were incubated with a mix of primary antibody (goat anti-IBA1, 1:1000 and rat anti Ki-67 1:500) in blocking solution overnight at 4°C. Next day, the tissue was washed three

times for 10 minutes in 1× PBS followed by incubation for 2 hours at room temperature in the dark with the mix of secondary antibodies, previously diluted in antibody buffer (2% horse serum in PBS, anti-goat, Alexa 647 (1:1000) and anti-rat Cy3, (1:500)). Sections were washed three times (1× PBS) for 10 minutes, placed in water and mounted in Aqua Poly Mount (Polysciences, Polysciences, Illinois).

In order to obtain an exact morphological analysis on microglia, stacks of images of the somatosensory cortex were acquired using a confocal laser scanning microscope (cLSM, LSM710) for which a 40×/1.0 objective (Plan-Aprochomat; 4 Oil DIC [UV] VIS-IR M 27) and appropriate emission filters were used. z-Series stacks of ramified brain microglia were captured at a resolution of 512 × 512 pixels (212.55 × 212.55 μm) at 1 μm intervals and processed using Zen Software (Carl Zeiss, Jena, Germany) and Fiji.[69] Images were acquired with a pixel time of 6.2 μs. Each z-series image stack included microglia with complete arbors; those with filaments that extended over the edges of the z-stack were omitted from the analysis.

4.3 | Image analysis

Two methods have been applied to quantify microglia morphology. First, a semi-manual method[70] was used for all time points. Second, a semi-automated method using the "Inflammation Index" duo of packages[35] That can be downloaded, and contributed to, on GitHub (https://github.com/BrainEnergyLab/Inflammation-Index) was used to compare results of the semi-manual approach across four time points.

For the semi-manual method, images were processed using Fiji software.[70] Only cells with a complete dendritic arbor were manually selected from the obtained stacks to be analyzed. A minimum of 25 and a maximum of 59 cells were obtained for each age group. Morphological analysis of microglial dendritic structure was made using five parameters: (1) total length of branch tree, (2) number of branches, (3) mean branch length, (4) number of each branch order, (5) mean area surveilled by each cell. In order to obtain the first four parameters, each microglial cell was converted to a topological skeleton depiction (Figure 4). The mean area surveilled by each cell was quantified by circumscribing the area outlined by the terminals of the longest dendrite in all directions. Besides the analysis of individual microglia, another two parameters were analyzed: the number of cells per mm^3 (microglial density-the measurement was performed by manually counting microglial cell bodies from each z-stack) and the frequency of microglia cell bodies close together, which we considered as a marker of proliferation.

The semi-automated method involved, firstly, formatting image stacks captured at the P5, P21, 58 weeks, and 110 weeks' time points for use with the "Inflammation Index" packages. This involved taking an average projection of the middle 10 μm of each image stack, before these were run through the "Microglia Morphology Analysis" Fiji plugin in order to semi-automatically generate microglial cell masks. For a full description of the methodology involved in this, please see.[35] Briefly, cell bodies were identified as local maxima before iterative thresholding was used to automatically generate masks around the soma. These masks were generated for a range of Target Mask Sizes (TMS; which serve as a guide for when to terminate the iterative thresholding procedure) and automated masks of the cell soma were also generated. All masks generated at all TMS values, as well as soma masks, were manually approved (ie, visually inspected) for analysis to ensure they captured the morphology of a single cell (ie, did not extend onto an adjacent cell) and accurately represented the cell soma. Finally, these masks were quantified across 43 different metrics. All steps were run after blinding ourselves to the animal identifiers and time points of image stacks using a random number generator to assign new values for these identifiers in order to ensure objectivity. Once mask quantification data had been collected, it was analyzed using the "Inflammation Index" R package.[35] Briefly, the R package takes a training data set containing two conditions and uses the area under the curve (AUC) of a receiver operating characteristic analysis to identify the metrics generated by the "Microglia Morphology Analysis" Fiji plugin that best discriminate between the conditions, where a larger AUC value denotes better discriminability. If any of these metrics are highly correlated (a Pearson's correlation coefficient above 0.9) the ones with the lowest AUC values are dropped, and a principal component Analysis (PCA) is run on the remaining metrics. The first principal component of the PCA is then used as a single composite metric that is best able to discriminate between the two treatment conditions. This is done for each TMS analyzed. The purpose of the composite metric is to provide a single value that represents how far along a spectrum of morphology a cell lies. In this article, we constructed composite metrics with the aim of distinguishing between two sets of developmental stages (P5 and 110 weeks, and P21 and 58 weeks). This provides advantages over choosing N metrics to use to compare the time points against one another for two main reasons. The first is that there is no bias introduced by requiring us to identify the metrics we want to analyses a priori as we instead consider all 43 automatically generated cell measurements for inclusion in the composite metric. The second advantage is that by outputting a single value for each comparison we reduce the risk of false positives resulting from multiple statistical comparisons. While we could apply post hoc corrections to account for this increase, this would reduce our statistical power to detect real changes.

We used receiver operating characteristic (ROC) analyses in order to identify which source metrics to include in the composite metrics. We ran an ROC analysis on each of the 43 source metrics and selected those with the highest area under the curve (AUC) values. The AUC value illustrates how effective a particular metric is at separating two conditions as we alter the metric's value. For example, in order to identify the source metrics to include in our composite metric comparing P5 and 110 weeks, we ran an ROC analysis on the "mean branch length." To do this we iterated through all of the possible "mean branch length" values, and for each value, computed the true positive rate (the number of cells below the value that were from P5) and false positive rate (the number of cells below the value that were not from P5). We then plotted the true positive rate and false positive rate for each value and then computed the AUC of this plot as a measure of how effective "mean branch length" is at identifying cells from P5 vs 110 weeks. We did this for each of the 43 metrics and chose the 5 with the greatest AUC values for inclusion in our P5 vs 110 weeks composite metric. We took the same approach for the P21 vs 58 weeks composite metric.

4.4 | Data analysis

For each mouse and each parameter, an average value was imported in GraphPad Prism 9.3 and/or Microsoft Excel to analyze the obtained parameters. One-way analysis of variance (ANOVA) test, with multiple compilation corrected by Tukey, with a 95% confidence interval was performed. In all figures the mean and SD (SD) are displayed. We used super plots to display the data, with large colored circles representing the mean obtained for each animal, while small points represent the values found for each parameter for individual cells analyzed for the animal in the same color. Statistical significance is depicted as follows: $*P < .05$, $**P < .01$ and $***P < .001$.

AUTHOR CONTRIBUTIONS

Sanziana Godeanu: Formal analysis (equal); investigation (equal); visualization (supporting). **Devin Clarke:** Investigation (equal); methodology (equal); software (lead); writing – original draft (equal). **Laura Stopper:** Data curation (equal); investigation (supporting); writing – original draft (supporting). **Alexandru-Florian Deftu:** Conceptualization (supporting); data curation (equal);

writing – review and editing (supporting). **Aurel Popa-Wagner:** Project administration (equal); validation (equal); writing – review and editing (equal). **Adrian Tudor Bălşeanu:** Project administration (supporting); resources (equal); validation (supporting); writing – review and editing (supporting). **Anja Scheller:** Conceptualization (equal); methodology (equal); project administration (equal); supervision (equal); writing – original draft (equal); writing – review and editing (equal). **Bogdan Catalin:** Conceptualization (equal); formal analysis (lead); funding acquisition (lead); investigation (equal); methodology (supporting); supervision (equal); validation (lead); visualization (lead); writing – original draft (equal); writing – review and editing (equal).

CONFLICT OF INTEREST STATEMENT

The authors declare that they have no competing interests.

ACKNOWLEDGMENT

DATA AVAILABILITY STATEMENT

The data sets used and/or analyzed during the current study are available from the corresponding author on reasonable request.

ETHICS STATEMENT

All experiments have been conducted according to The Federation of European Laboratory Animal Science Associations (FELASA) guidelines and have been approved by the Wellbeing of Experimental Animal Committee of the UMFCV (no 1.16/10.10.2019) and renew by the Veterinary Sanitary and Food Safety Directorates of Dolj county (14/29.03.2022), according to Romanian and European laws.

ORCID

Bogdan Catalin https://orcid.org/0000-0002-5706-8722

REFERENCES

1. Davalos D, Grutzendler J, Yang G, et al. ATP mediates rapid microglial response to local brain injury in vivo. *Nat Neurosci.* 2005;8(6):752-758. doi:10.1038/nn1472
2. Nimmerjahn A, Kirchhoff F, Helmchen F. Resting microglial cells are highly dynamic surveillants of brain parenchyma in vivo. *Science.* 2005;308(5726):1314-1318. doi:10.1126/science.1110647
3. Catalin B, Cupido A, Iancau M, Albu CV, Kirchhoff F. Microglia: first responders in the central nervous system. *Rom J Morphol Embryol.* 2013;54(3):467-472.
4. Weinhard L, di Bartolomei G, Bolasco G, et al. Microglia remodel synapses by presynaptic trogocytosis and spine head filopodia induction. *Nat Commun.* 2018;9(1):1228. doi:10.1038/s41467-018-03566-5
5. Catalin B, Stopper L, Balseanu T-A, Scheller A. The in situ morphology of microglia is highly sensitive to the mode of tissue fixation. *J Chem Neuroanat.* 2017;86:59-66. doi:10.1016/j.jchemneu.2017.08.007
6. Geirsdottir L, David E, Keren-Shaul H, et al. Cross-species single-cell analysis reveals divergence of the primate microglia program. *Cell.* 2019;179(7):1609-1622.e16. doi:10.1016/j.cell.2019.11.010
7. Davies DS, Ma J, Jegathees T, Goldsbury C. Microglia show altered morphology and reduced arborization in human brain during aging and Alzheimer's disease. *Brain Pathol.* 2017;27(6):795-808. doi:10.1111/bpa.12456
8. Migliarini S, Scaricamazza S, Valle C, Ferri A, Pasqualetti M, Ferraro E. Microglia morphological changes in the motor cortex of hSOD1(G93A) transgenic ALS mice. *Brain Sci.* 2021;11(6):807. doi:10.3390/brainsci11060807
9. Chechik G, Meilijson I, Ruppin E. Synaptic pruning in development: a computational account. *Neural Comput.* 1998;10(7):1759-1777.
10. Schafer DP, Lehrman EK, Kautzman AG, et al. Microglia sculpt postnatal neural circuits in an activity and complement-dependent manner. *Neuron.* 2012;74(4):691-705. doi:10.1016/j.neuron.2012.03.026
11. Harry GJ. Microglia during development and aging. *Pharmacol Ther.* 2013;139(3):313-326. doi:10.1016/j.pharmthera.2013.04.013
12. Riccomagno MM, Kolodkin AL. Sculpting neural circuits by axon and dendrite pruning. *Annu Rev Cell Dev Biol.* 2015;31:779-805.
13. Perry VH, Gordon S. Microglia. *Microbiol Spectr.* 2016;4(3):1-9. doi:10.1128/microbiolspec.MCHD-0003-2015
14. Badimon A, Strasburger HJ, Ayata P, et al. Negative feedback control of neuronal activity by microglia. *Nature.* 2020;586(7829):417-423. doi:10.1038/s41586-020-2777-8
15. Carvalho-Paulo D, Bento Torres Neto J, Filho CS, et al. Microglial morphology across distantly related species: phylogenetic, environmental and age influences on microglia reactivity and surveillance states [review]. *Front Immunol.* 2021;12(2330):683026. doi:10.3389/fimmu.2021.683026
16. Wlodarczyk A, Holtman IR, Krueger M, et al. A novel microglial subset plays a key role in myelinogenesis in developing brain. *EMBO J.* 2017;36(22):3292-3308. doi:10.15252/embj.201696056
17. Butovsky O, Weiner HL. Microglial signatures and their role in health and disease. *Nat Rev Neurosci.* 2018;19(10):622-635. doi:10.1038/s41583-018-0057-5
18. Réu P, Khosravi A, Bernard S, et al. The lifespan and turnover of microglia in the human brain. *Cell Rep.* 2017;20(4):779-784. doi:10.1016/j.celrep.2017.07.004
19. Askew K, Li K, Olmos-Alonso A, et al. Coupled proliferation and apoptosis maintain the rapid turnover of microglia in the adult brain. *Cell Rep.* 2017;18(2):391-405. doi:10.1016/j.celrep.2016.12.041
20. Cronk JC, Filiano AJ, Louveau A, et al. Peripherally derived macrophages can engraft the brain independent of irradiation and maintain an identity distinct from microglia. *J Exp Med.* 2018;215(6):1627-1647. doi:10.1084/jem.20180247
21. Lund H, Pieber M, Parsa R, et al. Fatal demyelinating disease is induced by monocyte-derived macrophages in the absence of

TGF-β signaling. *Nat Immunol.* 2018;19(5):1-7. doi:10.1038/s41590-018-0091-5

22. Ginhoux F, Greter M, Leboeuf M, et al. Fate mapping analysis reveals that adult microglia derive from primitive macrophages. *Science.* 2010;330(6005):841-845. doi:10.1126/science.1194637

23. Goldmann T, Wieghofer P, Jordão MJ, et al. Origin, fate and dynamics of macrophages at central nervous system interfaces. *Nat Immunol.* 2016;17(7):797-805. doi:10.1038/ni.3423

24. de Oliveira TCG, Carvalho-Paulo D, de Lima CM, et al. Long-term environmental enrichment reduces microglia morphological diversity of the molecular layer of dentate gyrus. *Eur J Neurosci.* 2020;52(9):4081-4099. doi:10.1111/ejn.14920

25. Hefendehl JK, Neher JJ, Sühs RB, Kohsaka S, Skodras A, Jucker M. Homeostatic and injury-induced microglia behavior in the aging brain. *Aging Cell.* 2014;13(1):60-69. doi:10.1111/acel.12149

26. Tremblay M, Zettel ML, Ison JR, Allen PD, Majewska AK. Effects of aging and sensory loss on glial cells in mouse visual and auditory cortices. *Glia.* 2012;60(4):541-558. doi:10.1002/glia.22287

27. Damani MR, Zhao L, Fontainhas AM, Amaral J, Fariss RN, Wong WT. Age-related alterations in the dynamic behavior of microglia. *Aging Cell.* 2011;10(2):263-276. doi:10.1111/j.1474-9726.2010.00660.x

28. Sierra A, Gottfried-Blackmore AC, McEwen BS, Bulloch K. Microglia derived from aging mice exhibit an altered inflammatory profile. *Glia.* 2007;55(4):412-424. doi:10.1002/glia.20468

29. Lopes KO, Sparks DL, Streit WJ. Microglial dystrophy in the aged and Alzheimer's disease brain is associated with ferritin immunoreactivity. *Glia.* 2008;56(10):1048-1060. doi:10.1002/glia.20678

30. Santello M, Calì C, Bezzi P. Gliotransmission and the tripartite synapse. *Adv Exp Med Biol.* 2012;970:307-331. doi:10.1007/978-3-7091-0932-8_14

31. Perry VH, Matyszak MK, Fearn S. Altered antigen expression of microglia in the aged rodent CNS. *Glia.* 1993;7(1):60-67. doi:10.1002/glia.440070111

32. Franceschi C, Capri M, Monti D, et al. Inflammaging and anti-inflammaging: a systemic perspective on aging and longevity emerged from studies in humans. *Mech Ageing Dev.* 2007;128(1):92-105. doi:10.1016/j.mad.2006.11.016

33. Liu YU, Ying Y, Li Y, et al. Neuronal network activity controls microglial process surveillance in awake mice via norepinephrine signaling. *Nat Neurosci.* 2019;22(11):1771-1781. doi:10.1038/s41593-019-0511-3

34. Wake H, Moorhouse AJ, Jinno S, Kohsaka S, Nabekura J. Resting microglia directly monitor the functional state of synapses in vivo and determine the fate of ischemic terminals. *J Neurosci.* 2009;29(13):3974-3980. doi:10.1523/jneurosci.4363-08.2009

35. Clarke D, Crombag HS, Hall CN. An open-source pipeline for analysing changes in microglial morphology. *Open Biol.* 2021;11(8):210045. doi:10.1098/rsob.210045

36. Cunningham CL, Martínez-Cerdeño V, Noctor SC. Microglia regulate the number of neural precursor cells in the developing cerebral cortex. *J Neurosci.* 2013;33(10):4216-4233. doi:10.1523/jneurosci.3441-12.2013

37. Ajami B, Bennett JL, Krieger C, Tetzlaff W, Rossi FM. Local self-renewal can sustain CNS microglia maintenance and function throughout adult life. *Nat Neurosci.* 2007;10(12):1538-1543. doi:10.1038/nn2014

38. Saijo K, Glass CK. Microglial cell origin and phenotypes in health and disease. *Nat Rev Immunol.* 2011;11(11):775-787. doi:10.1038/nri3086

39. Cayre M, Canoll P, Goldman JE. Cell migration in the normal and pathological postnatal mammalian brain. *Prog Neurobiol.* 2009;88(1):41-63. doi:10.1016/j.pneurobio.2009.02.001

40. Paredes MF, James D, Gil-Perotin S, et al. Extensive migration of young neurons into the infant human frontal lobe. *Science.* 2016;354(6308):aaf7073. doi:10.1126/science.aaf7073

41. Lier J, Ondruschka B, Bechmann I, Dreßler J. Fast microglial activation after severe traumatic brain injuries. *Int J Leg Med.* 2020;134(6):2187-2193. doi:10.1007/s00414-020-02308-x

42. Stopper L, Bălşeanu T-A, Cătălin B, Rogoveanu O-C, Mogoantă L, Scheller A. Microglia morphology in the physiological and diseased brain – from fixed tissue to in vivo conditions. *Rom J Morphol Embryol.* 2018;59(1):7-12.

43. Chu T, Zhang YP, Tian Z, et al. Dynamic response of microglia/macrophage polarization following demyelination in mice. *J Neuroinflammation.* 2019;16(1):188. doi:10.1186/s12974-019-1586-1

44. Nikodemova M, Kimyon RS, De I, Small AL, Collier LS, Watters JJ. Microglial numbers attain adult levels after undergoing a rapid decrease in cell number in the third postnatal week. *J Neuroimmunol.* 2015;278:280-288. doi:10.1016/j.jneuroim.2014.11.018

45. Irintchev A, Rollenhagen A, Troncoso E, Kiss JZ, Schachner M. Structural and functional aberrations in the cerebral cortex of tenascin-C deficient mice. *Cereb Cortex.* 2005;15(7):950-962. doi:10.1093/cercor/bhh195

46. Spangenberg E, Severson PL, Hohsfield LA, et al. Sustained microglial depletion with CSF1R inhibitor impairs parenchymal plaque development in an Alzheimer's disease model. *Nat Commun.* 2019;10(1):3758. doi:10.1038/s41467-019-11674-z

47. Knox EG, Aburto MR, Clarke G, Cryan JF, O'Driscoll CM. The blood–brain barrier in aging and neurodegeneration. *Mol Psychiatry.* 2022;27(6):2659-2673. doi:10.1038/s41380-022-01511-z

48. Rotaru-Zavaleanu AD, Neacşu AI, Neacşu AD, et al. Effects of acute sepsis on cellular dynamics and amyloid formation in a mouse model of Alzheimer's disease. *Curr Issues Mol Biol.* 2022;44(9):3822-3834. doi:10.3390/cimb44090262

49. Morega S, Gresita A, Mitran SI, et al. Cerebrolysin use in patients with liver damage-a translational study. *Life (Basel).* 2022;12(11):1791. doi:10.3390/life12111791

50. Morega S, Cătălin B, Simionescu CE, Sapalidis K, Rogoveanu I. Cerebrolysin prevents brain injury in a mouse model of liver damage. *Brain Sci.* 2021;11(12):1622. doi:10.3390/brainsci11121622

51. Rosu G-C, Catalin B, Balseanu TA, et al. Inhibition of aquaporin 4 decreases amyloid Aβ40 drainage around cerebral vessels. *Mol Neurobiol.* 2020;57:4720-4734. doi:10.1007/s12035-020-02044-8

52. Fendrick SE, Xue QS, Streit WJ. Formation of multinucleated giant cells and microglial degeneration in rats expressing a mutant Cu/Zn superoxide dismutase gene. *J Neuroinflammation.* 2007;4:9. doi:10.1186/1742-2094-4-9

53. Cojocaru A, Burada E, Bălşeanu AT, et al. Roles of microglial ion channel in neurodegenerative diseases. *J Clin Med.* 2021;10(6):1239. doi:10.3390/jcm10061239

54. Stojiljkovic MR, Ain Q, Bondeva T, Heller R, Schmeer C, Witte OW. Phenotypic and functional differences between senescent and aged murine microglia. _Neurobiol Aging_. 2019; 74:56-69. doi:10.1016/j.neurobiolaging.2018.10.007

55. Stence N, Waite M, Dailey ME. Dynamics of microglial activation: a confocal time-lapse analysis in hippocampal slices. _Glia_. 2001;33(3):256-266.

56. Donat CK, Scott G, Gentleman SM, Sastre M. Microglial activation in traumatic brain injury. _Front Aging Neurosci_. 2017;9: 208. doi:10.3389/fnagi.2017.00208

57. Surugiu R, Catalin B, Dumbrava D, et al. Intracortical administration of the complement C3 receptor antagonist trifluoroacetate modulates microglia reaction after brain injury. _Neural Plast_. 2019;2019:9. doi:10.1155/2019/1071036

58. Osiac E, Mitran SI, Manea CN, et al. Optical coherence tomography microscopy in experimental traumatic brain injury. _Microsc Res Tech_. 2021;84(3):422-431. doi:10.1002/jemt.23599

59. Anton R, Ghenghea M, Ristoiu V, et al. Potassium channels Kv1.3 and Kir2.1 but not Kv1.5 contribute to BV2 cell line and primary microglial migration. _Int J Mol Sci_. 2021;22(4):2081.

60. Streit WJ, Braak H, Xue QS, Bechmann I. Dystrophic (senescent) rather than activated microglial cells are associated with tau pathology and likely precede neurodegeneration in Alzheimer's disease. _Acta Neuropathol_. 2009;118(4):475-485. doi:10.1007/s00401-009-0556-6

61. Streit WJ, Mrak RE, Griffin WS. Microglia and neuroinflammation: a pathological perspective. _J Neuroinflammation_. 2004; 1(1):14. doi:10.1186/1742-2094-1-14

62. Streit WJ, Sammons NW, Kuhns AJ, Sparks DL. Dystrophic microglia in the aging human brain. _Glia_. 2004;45(2):208-212. doi:10.1002/glia.10319

63. Streit WJ. Microglial senescence: does the brain's immune system have an expiration date? _Trends Neurosci_. 2006;29(9):506-510. doi:10.1016/j.tins.2006.07.001

64. Korotzer AR, Pike CJ, Cotman CW. Beta-amyloid peptides induce degeneration of cultured rat microglia. _Brain Res_. 1993; 624(1–2):121-125. doi:10.1016/0006-8993(93)90068-x

65. Brawek B, Schwendele B, Riester K, et al. Impairment of in vivo calcium signaling in amyloid plaque-associated microglia. _Acta Neuropathol_. 2014;127(4):495-505. doi:10.1007/s00401-013-1242-2

66. Olmedillas Del Moral M, Asavapanumas N, Uzcátegui NL, Garaschuk O. Healthy brain aging modifies microglial calcium signaling in vivo. _Int J Mol Sci_. 2019;20(3):589. doi:10.3390/ijms20030589

67. Streit WJ, Sparks DL. Activation of microglia in the brains of humans with heart disease and hypercholesterolemic rabbits. _J Mol Med (Berl)_. 1997;75(2):130-138.

68. Jung S, Aliberti J, Graemmel P, et al. Analysis of fractalkine receptor CX(3)CR1 function by targeted deletion and green fluorescent protein reporter gene insertion. _Mol Cell Biol_. 2000; 20(11):4106-4114.

69. Schindelin J, Arganda-Carreras I, Frise E, et al. Fiji: an open-source platform for biological-image analysis. _Nat Methods_. 2012;9(7):676-682. doi:10.1038/nmeth.2019

70. Meijering E, Jacob M, Sarria JC, Steiner P, Hirling H, Unser M. Design and validation of a tool for neurite tracing and analysis in fluorescence microscopy images. _Cytometry A_. 2004;58(2): 167-176. doi:10.1002/cyto.a.20022